Research Article

Changes in Amorphous and Crystalline Phases of Ion-exchange Membranes MA-41P and MK-40 in the Separation of Industrial Solutions by Electrodeionization and Electrodialysis Methods

Sergey Lazarev, Konstantin Shestakov* and Maxim Mikhaylin
Department of Mechanics and Engineering Graphics, Technological Institute, Tambov State Technical University, Tambov, Russia

Irina Khorokhorina
Department of Nature Management and Environment Protection, Technological Institute, Tambov State Technical University, Tambov, Russia

* Corresponding author. E-mail: shestakov.kv@mail.tstu.ru DOI: 10.14416/j.asep.2024.12.002
Received: 14 September 2024; Revised: 31 October 2024; Accepted: 20 November 2024; Published online: 12 December 2024

Abstract
The interest in studying the structure of ion-exchange membranes is degree of crystallinity, the interplanar distance and size of crystallites and other characteristics. This work aimed to study the change in structural characteristics of ion-exchange membranes MA-41P and MK-40 during electrodeionization and electrodialysis using X-ray diffraction (XRD) analysis and differential scanning calorimetry (DSC). For these processes, multicomponent solution model was used, which was similar in composition to industrial solutions used in galvanic production. It contained $CuSO_4$, $CoSO_4$, $CdSO_4$, $Fe(NO_3)_3$ and $Ni(NO_3)_2$ with different initial concentration. As a result of the study, it was found that mechanical, chemical and thermal loads lead to the formation of defects and the gradual destruction of the membrane structure. The membrane becomes less selective, the ion transmission becomes less controllable, and undesirable reactions with the processed medium occur. The observed deviation of the diffraction angles at the crystalline peaks of water-saturated and working membrane samples indicates the sensitivity of macromolecules to mechanical and thermal loads arising under cyclic operation. This is due to a change in structural ordering, polymer matrix amorphization and intermolecular interactions within the membrane structure. A comparative analysis of the membrane structural characteristics after the separation processes has shown that the structure of the cation-exchange membrane MK-40 contains a larger percentage by 2–9 of the crystalline phase compared to the anion-exchange membrane MA-41P, which provides it with greater mechanical and chemical resistance during operation. In contrast, the anion-exchange membrane MA-41P is more amorphous and has a stronger absorption capacity.

Keywords: Electrodeionization, Electrodialysis, Galvanic production, Industrial solutions, Membrane, Structure

1 Introduction

Ion-exchange membranes are semipermeable materials that selectively allow ions of a certain charge to pass through. They are used in many technological processes, including food production, fuel cells, water desalination systems, etc. [1]–[8]. Ion-exchange membranes usually consist of a polymer matrix with functional groups included in it. These functional groups determine the properties of the membrane – anionic or cationic [9].

Polymer matrices can be both amorphous and crystalline, but it is the amorphous phase that plays a key role in their functionality, while the crystalline phase characterizes the strength properties [10]. Therefore, changing the ratio of crystallinity and amorphism in ion-exchange membranes affects their characteristics and efficiency, as well as selectivity for

ions. For example, membranes with a higher degree of amorphism, as a rule, have higher ionic conductivity. Membranes with a more crystalline structure have greater mechanical strength. Higher crystallinity is often associated with lower susceptibility to chemical attack, as the ordered structure is less susceptible to interactions with aggressive substances. Amorphous phases usually have large intermolecular spatial gaps and a higher specific surface area, which improves the adsorption of solute ions and facilitates their penetration into the membrane. This is especially important in ion-exchange processes. It is important to note that amorphous membrane structures can be more susceptible to chemical and thermal decomposition [11].

Crystallinity and amorphism in the structure of ion-exchange membranes depend on several factors. One of them is the chemical composition of the membrane, which can be made using various polymeric materials such as polyethylene, polytetrafluoroethylene, polyvinyl chloride, etc. These materials have different degrees of crystallinity (DC) depending on their chemical structure and production method [12]. Another factor that can affect DC is the membrane production method. Faster production methods result in a more amorphous structure [12]. Cross-linking and surface modification can also affect crystallinity and amorphism. For example, the introduction of functional groups such as sulfonate or carboxyl groups can increase amorphism [12]. In addition, the absorption of water and ions by the membrane can affect its crystallinity, since hydration and interaction of the membrane with ions can destroy the crystalline structure of the membrane, increasing amorphism [13].

The study of crystalline and amorphous phases and other structural characteristics of ion-exchange membranes allows for improved membrane efficiency in various fields of application and also promotes the development of more advanced materials for the needs of modern science and industry. Currently, various methods can be used to study the structure of ion-exchange membranes. For example, X-ray diffraction (XRD) can be used to study the amorphous and crystalline phases in the membrane structure. Amorphous phases appear as broad, low-intensity halos, while crystalline phases appear as sharp peaks [14]. Differential scanning calorimetry (DSC) is used to study the thermal characteristics, including the melting point and glass transition temperature of the polymeric materials from which the ion-exchange membrane matrix is made [15], [16]. Optical and electron microscopy can be used to visualize and study the morphology and structure of membranes at the micro- and nanoscale [17]. Infrared or nuclear magnetic resonance spectroscopy can be used to understand the interactions between ions and the polymer matrix [18], [19]. In some cases, when membranes are subjected to modification and the membrane's strength data is no longer relevant, mechanical methods are used to further examine the membrane structure for compressive or tensile strength, as well as to assess the impact of such effects on the membrane's durability [20].

The data obtained in such studies can be used for a wide range of tasks, for example, to optimize the structure and properties of existing membranes, develop new materials with specified characteristics, and predict the behavior of membranes under various operating conditions [21]–[23]. Therefore, the purpose of this work was to study the change in a number of structural characteristics of ion-exchange membranes during electrodeionization (EDI) and electrodialysis (ED) using XRD and DSC methods.

2 Materials and Methods

2.1 *Objects of research and methods of separation of solutions*

2.1.1 The tested membranes

The ion-exchange membranes MA-41P and MK-40 (Shchekinoazot, Russia, batch production date 2023) were selected for the study. These membranes are a mechanical composition consisting of particles of ground granulated ion exchangers of 5 to 50 μm in size, pressed into a matrix of low-pressure polyethylene. Polyamide reinforcing fabric is introduced into their structure to increase mechanical strength. Table 1 provides a brief description of the tested membranes [24].

Ion-exchange membranes MK-40 and MA-41P are used in a number of industrial processes, ensuring high efficiency and quality of products. This series includes water treatment and desalination, food industry (purification and concentration of various juices and wines), chemical industry (purification of industrial wastewater from heavy metal ions and their concentration).

Table 1: Characteristics of ion-exchange membranes.

Membrane	Thickness, mm	Tensile Strength, MPa, No less	Surface Electrical Resistance, $\Omega \cdot cm^{-2}$, No more	Ionic Group	Counter Ion	Inert Binder	Reinforcing Fabric
MK-40	0.3 – 0.5	11.9	10.0	SO_3H	Na^+	Polyethylene	Polyamide
MA-41P		11.0	11.0	$N(CH_3)$	Cl^-		

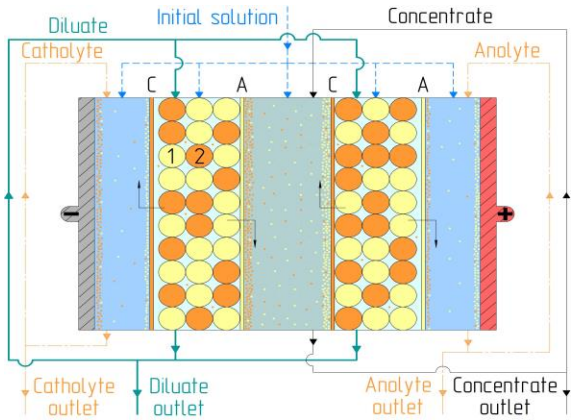

Figure 1: Schematic representation of the EDI apparatus: 1 – anion-exchange resin particles, 2 – cation-exchange resin particles.

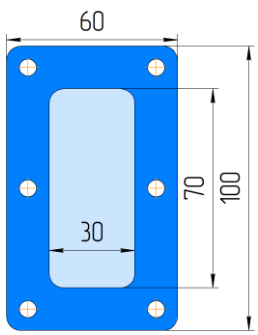

Figure 2: Shape and overall dimensions of the EDI module.

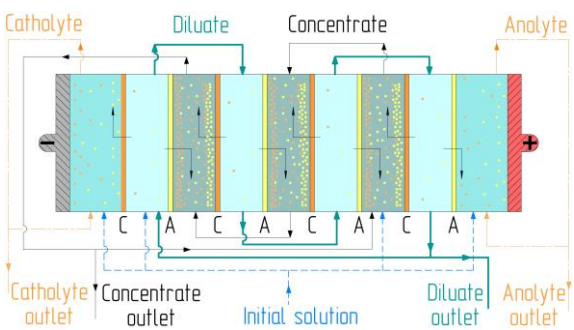

Figure 3: Schematic representation of the electrodialysis apparatus.

2.1.2 Methods of separation of solutions and apparatus

The study of changes in the structure of ion-exchange membranes resulting from the separation of industrial solutions by the EDI method was carried out using a setup whose general operating diagram is shown in Figure 1.

The EDI module, the overall dimensions of which are shown in Figure 2, consisted of two parts of the housing with channels for solutions, two electrodes, two anion-exchange and two cation-exchange membranes with an active area of 0.0021 m^2 each, three intermembrane and two near-electrode gaskets, inlet and outlet fittings for solutions. The connection of the module elements was made using a bolted connection. The composition of the apparatus was as follows: containers for diluate, concentrate, anolyte and catholyte, EDI module, pumps for feeding solutions into the EDI module chambers, and a laboratory power supply.

The ED separation process was carried out on a laboratory apparatus, shown schematically in Figure 3. It included an electrodialysis cell, a laboratory power supply unit, and lines for the circulation of diluate, concentrate, anolyte, and catholyte with auxiliary equipment, including solution containers, diaphragm pneumatic pumps, pressure gauges, flow meters, inlet and outlet valves, etc.

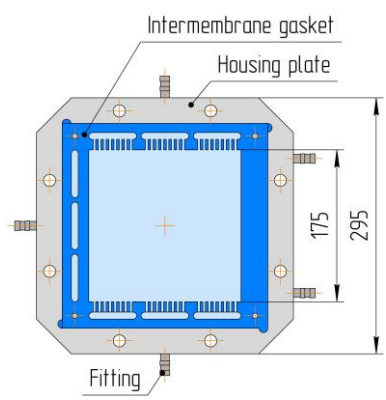

Figure 4: Shape and overall dimensions of the electrodialysis cell.

The cell was assembled from two pressure plates with channels for solutions, two electrodes laid in alternating order, four anion-exchange and four cation-exchange membranes of the above-mentioned brands with an active area of 0.0306 m^2 each, seven intermembranes and two near-electrode gaskets, inlet and outlet nozzles for solutions. The overall dimensions of the cell are shown in Figure 4. The assembly was carried out using a bolted connection.

2.1.3 Membrane preparation and experimental operating parameters

To study the changes in the structure of ion-exchange membranes, four types of samples were used: initial dry, initial water-saturated, working after EDI and working after ED. All samples of MA-41P and MK-40 membranes for XRD and DSC studies were taken from industrially produced sheets. The initial dry membrane samples were not pre-activated and were cut out 5×5 mm in size directly from the membrane sheets. Half of them were left in distilled water for 24 h in a dark place to obtain the initial water-saturated samples. In parallel, working membranes were cut out from industrial sheets for direct use in the EDI and ED installations.

Before the EDI and ED processes, the membranes underwent a preparatory activation procedure in a 0.6 M NaCl solution for 24 h in a dark place. After all EDI and ED processes were completed, 5×5 mm samples were cut out from the central part of the active zone of the spent membranes. Drying of water-saturated and spent samples was not allowed before the XRD and DSC studies.

Also for the EDI process, the ion-exchange resins were activated. For this purpose, an excess volume of a 4% NaCl solution was placed in 2 separate containers with anion-exchange AB-17-8 and cation-exchange KU-2-8 resins for 4 h to saturate the resins with Na^+ and Cl^- ions. During this time, the solution was renewed twice. This concentration of the preparatory solution was chosen to prevent damage to the resin due to osmotic shock caused by intense ion exchange.

For the EDI process, model multicomponent solutions were used, which were similar in composition to industrial solutions used in galvanic production. They contained $CuSO_4$, $CoSO_4$ and $CdSO_4$ with an initial concentration of 63, 53 and 37 mg/dm^3, respectively. The operating parameters of the experiment were: current density – from 5 to 25 A/m^2, average flow rate of the separated solution in each section of the unit – from $0.16 \cdot 10^{-5}$ to $0.17 \cdot 10^{-5}$ m^3/s, duration of one experiment – 3600 s, initial volume of solutions – $2 \cdot 10^{-3}$ m^3 in each section, width of the intermembrane channel – $1 \cdot 10^{-3}$ m. A total of 16 such experiments were conducted.

The model multicomponent solutions used in the ED separation process, similar to industrial solutions of galvanic production, contained CuSO4, $Fe(NO_3)_3$ and $Ni(NO_3)_2$ with an initial concentration of 350, 700 and 520 mg/dm^3, respectively. The operating parameters of the experiment were: current density – from 10 to 40 A/m^2, average flow rate of the separated solution in each section of the setup – from $8 \cdot 10^{-5}$ to $9 \cdot 10^{-5}$ m^3/s, duration of one experiment – 3600 s, initial volume of solutions – $5 \cdot 10^{-3}$ m^3 in each section, width of the intermembrane channel – $1 \cdot 10^{-3}$ m. A total of 16 such experiments were carried out, as in the case of using EDI.

The choice of the initial solutions is due to the fact that all the ions mentioned in the article are present in wastewater and industrial solutions in the form of various compounds. Cu^{2+} cations enter wastewater due to the galvanic deposition of copper on holes in printed circuit boards for subsequent application of a metal resist and in copper etching processes. The presence of Ni^{2+} cations is due to the fact that nickel is most often used as a sublayer for other metal-deposited coatings. For example, it is effective as a barrier sublayer to prevent diffusion between copper and other metals. Fe^{3+} cations are present in industrial solutions and wastewater as a result of copper etching processes. or copper, nickel-iron alloys and steel in the production of printed circuit boards, metal photolithography and metal finishing. The presence of Cd^{2+} and Co^{2+} cations is due to the galvanic processes of cadmium plating and cobalt plating. The presence of SO_4^{2-} and NO_3^- anions in the effluents can be explained, for example, by the use of $CuSO_4$ in the processes of galvanic deposition of copper and NH_4NO_3 to accelerate the etching process.

The choice of electric current densities from 10 to 40 A/m^2 is due to the process being carried out in super-limit current modes. Such modes are aimed at intensifying the processes of electromembrane purification, which is beneficial to the industry. Despite the fact that in this case energy costs increase, the super-limit current mode allows for a significant increase in the efficiency of removing target substances from solutions. This ultimately offsets the extra costs of electricity [25].

The selected flow rate is determined by the experimental setup designs and the average values used in industrial setups. It should be noted that for the EDI setup, the flow rate values were scaled due to their small size after a comparative analysis with industrial setups.

2.2 *Methods of membrane study*

The main interest in studying the structure of ion-exchange membranes is DC, the interplanar distance of crystallites, their size, and the heat flow released from 1 mg of sample mass. This is due to the fact that during cyclic use of membranes, these characteristics are subject to change first of all. They can be used to evaluate the structural transformations occurring in the membrane.

The X-ray diffraction and DSC methods are widely used to study the structure of ion-exchange membranes. Thus, X-ray diffraction is used to study the morphology and heterogeneity of membranes, allowing one to study the shape and size of crystallites and their distribution in the membrane structure. These methods can also be used to assess the interaction of the membrane with water and the effect of this factor on transport properties. The study of these aspects can help in assessing the mechanical and chemical properties of the membrane. The DSC method is used to determine the melting point of membrane components and to study the thermodynamic processes occurring in the membrane when heated. This allows one to understand the stability of materials at different temperatures.

The study of changes in the crystallinity and amorphism of the membrane structure was carried out using an X-ray diffractometer "Difray-401" (JSC *Nauchnie pribory*, Russia). The Bragg-Brentano focusing method was used, which allows the recording of scattered X-ray radiation from different areas of the sample. CuKα radiation with a wavelength of 1.54 Å was used for the study. The range of angles 2θ was from 7 to 60°, which provided a large amount of information on the structure of ion-exchange membranes.

DSC studies were carried out using a thermal analyzer "STA 449 F3 Jupiter" (Netzsch Geratebau GmbH, Germany), in crucibles made of aluminum oxide Al_2O_3, the samples were heated in air in the range from 30 to 500 °C at a rate of 10 °C/min. Such heating parameters and experimental conditions made it possible to study the behavior of the samples at different temperatures and evaluate their thermal properties. These data were important for further understanding of the thermochemical processes and material behavior in the samples studied.

Experimental studies of membrane structure using X-ray diffraction and differential scanning calorimetry (DSC) were repeated three times for each type of membrane sample to ensure the stability of the results.

2.3 *Processing of study results*

The experimental data obtained as a result of the studies using the XRD and DSC methods were processed in the OriginPro 2024b software package for a more detailed analysis and determination of the structural characteristics of the membranes, as well as a number of parameters of the destruction process. The use of built-in algorithms for analyzing the location and shape of peaks made it possible to more accurately determine the structural features of the membranes and estimate the parameters of their destruction as a result of the operation.

For the analysis, the main parameters of the diffraction peaks obtained from the experimental data were used. They made it possible to calculate the size of the interplanar distance in crystallites, the size of the crystallites and the DC of the membrane samples under study.

To determine the crystallographic parameters of reflections at different angles, the Bragg equation was used, which is based on the principle of interference of X-rays reflected from atomic planes in a crystal. The Bragg equation has the following form Equation (1) [26]:

$$d = \lambda(2\sin\theta)^{-1}, \quad (1)$$

where λ – the wavelength of X-ray radiation, Å; θ – the diffraction angle, °.

To determine the size of crystallites in the membrane structure, the Scherrer formula [27] was used, which is based on the analysis of the diffraction peak profile [Equation (2)]:

$$L = \frac{K_1\lambda}{\beta\cos\theta}, \quad (2)$$

where K_1 – the dimensionless particle shape factor (taken equal to 0.9 [28]); λ – the wavelength of X-ray

radiation, nm; β – the width of the reflection at half-maximum (half-width) of the peak, °.

To determine the degree of crystallinity (DC) of the polymer material, the Aggarwal-Till method was used [29]. The essence of this method is to separate reflections associated with the crystalline and amorphous phases in the diffraction pattern of the polymer material. Then, the DC was calculated using the relationship:

$$DC = \frac{I_k}{I_k + K_2 \cdot I_a} \cdot 100\%, \quad (3)$$

where I_k – the integral intensity of the crystalline phase; K_2 – the coefficient taking into account the polarization and monochromatic factors (adopted equal to 0.556 [30]); I_a – the integral intensity of the amorphous phase.

3 Results and Discussion

3.1 *Results of the study using the XRD*

During the X-ray structural study of ion-exchange membranes MA-41P and MK-40, diffraction patterns of the initial dry and water-saturated membrane samples, as well as samples after the EDI and ED processes were obtained (Figures 5 and 6). It should be noted that all diffraction patterns are presented after background subtraction.

The diffraction pattern of the initial dry sample of the MA-41P membrane (Figure 5a) is characterized by the presence of two clearly defined peaks at 2θ angles of 22.07 and 24.47°. Such angle values are typical for the crystalline phase of polyethylene and polyamide included in the samples. A small area with weakly defined peaks at 2θ angles greater than 35° is also observed in the diffraction patterns. The interplanar distance in the crystallites of the sample varies between 3.63–4.03 Å. The maximum crystallite size of this sample is 3.47 Å. The amorphous phase of the membrane is expressed by one halo across the entire width of the diffraction pattern with a maximum intensity of 60 conventional units. The DC of this sample calculated using the formula Equation (3) was 45.06%.

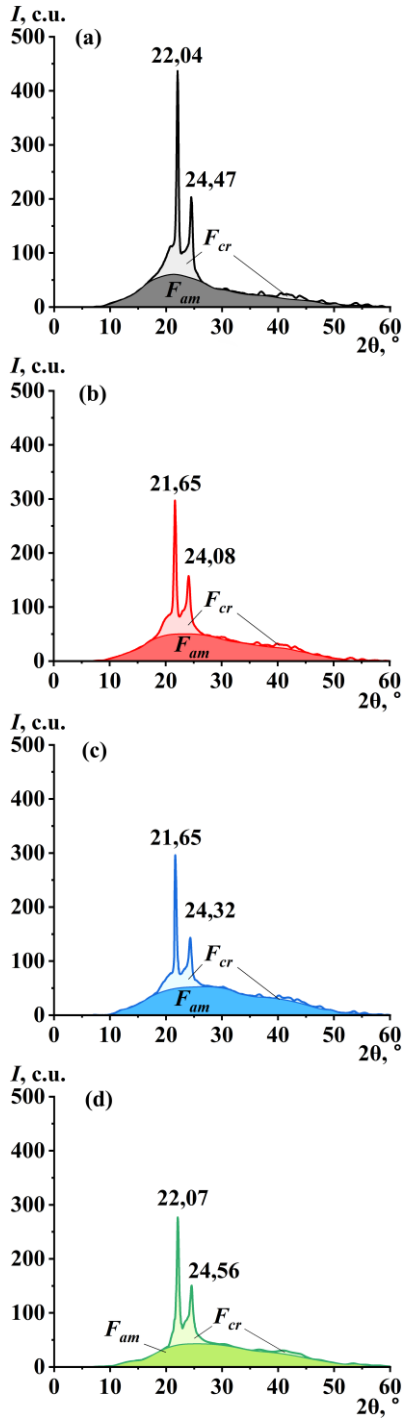

Figure 5: X-ray diffraction patterns of MA-41P membrane samples after background subtraction: *a* – initial dry; *b* – initial water-saturated; *c* – after EDI; *d* – after ED.

The saturation of the initial sample with water resulted in some structural changes. This is expressed in the shift of pronounced crystalline peaks (Figure 5(b)) towards smaller 2θ angles to 21.65 and 24.08°, respectively. In addition, there was a decrease in the absolute intensity of these peaks by about 30%. The interplanar distance in the crystallites slightly increased on average and varied in the range of 3.69 – 4.09 Å. These observations can be explained by the fact that during water saturation, water molecules penetrate the membrane structure, and the ions contained in the membrane begin to bind with water molecules. This leads to an increase in the membrane volume and creates defects and inhomogeneities in its crystalline phase, which ultimately leads to a blurring of the peaks and a decrease in their intensity [31]. The amorphous halo was similar to the halo of the dry sample, but the maximum intensity was lower – 50 c.u. The DC of the water-saturated sample decreased almost and amounted to 39.17%.

The diffraction pattern of the working membrane sample after EDI (Figure 5(c)) shows peaks at diffraction angles of 21.65 and 24.32°. It shows a shift of the second peak to the right compared to the water-saturated sample, which is associated with a decrease in the interplanar distance in the crystallites to 3.65 Å. The DC of this sample has significantly decreased compared to the dry and water-saturated samples to 32.75%. This diffraction pattern is also characterized by one amorphous halo, the maximum intensity of which was slightly higher than that of the water-saturated sample – slightly more than 52 c.u.

Analysis of the MA-41P membrane sample after ED separation allowed us to establish crystalline peaks at angles of 22.07 and 24.56° (Figure 5(d)). Their intensity and width are comparable with similar parameters of the spent membrane sample after EDI, while the DC was slightly higher and amounted to 38.38%. The interplanar distance in the crystallites decreased and varied in the range of 3.62–4.02 Å. The maximum intensity of the amorphous halo on the diffraction pattern is the lowest among all MA-41P membrane samples and is equal to 42 c.u.

Table 2 shows the ratio of a number of diffractometric parameters of the anion-exchange membrane MA-41P. As a result of a general analysis of the obtained experimental data, it can be explained as follows. The shift of the crystallinity peaks towards larger diffraction angles and the decrease in the overall intensity in the diffraction patterns of the working samples are due to changes in the structure of the crystalline phase of the membranes. This is probably caused by the preparatory procedures of membrane activation and compression and the actual conduct of the experiments. These procedures could lead to compaction of the membranes and a subsequent change in the interactions between molecules, which affected the parameters of the crystalline phase [32]. The decrease in the maximum intensity of the amorphous halo and, at the same time, the increase in the integral intensity is due to the saturation of the ion-exchange resin particles in the membrane structure with moisture.

Water saturation and the implementation of EDI and ED processes had a greater effect on the crystalline phase of the MA-41P membrane structure than on the amorphous one. This conclusion was led by a decrease in the DC of the membrane samples. In addition, this thesis is confirmed by a stronger decrease in the intensity of crystalline peaks compared to the maximum and integral intensities of the amorphous halo, as well as a decrease in the size of crystallites in the samples.

Next, the data obtained for the MK-40 cation-exchange membrane were analyzed. The diffraction patterns of each sample show two distinct peaks characterizing crystallinity due to the presence of polyethylene and polyamide in the membrane structure, two amorphous halos with angle ranges greater than 15, and an area with weakly expressed crystalline peaks. Based on the membrane composition, it can be assumed that the crystallinity peaks are due to polyethylene, which acts as a binder for combining ion-exchange resins, and polyamide, which acts as a substrate to impart mechanical strength to the membrane. The amorphous part of the membrane is an ion-conducting material made of ion-exchange resins based on a styrene copolymer.

Thus, the diffraction pattern of the initial dry membrane sample (Figure 6(a)) shows two clear crystalline peaks at 2θ angles of 21.07 and 23.44° with an interplanar distance of 4.21 and 3.79 Å, respectively, as well as several weakly expressed crystalline peaks in the 2θ angle range from 34 to 45° and from 52 to 56°. In addition, unlike the anion-exchange membrane MA-41P, the diffraction pattern of the dry initial MK-40 sample shows two amorphous halos in the angle ranges from 10 to 35° and 35 to 60°. These areas correspond to the particles of the cation-exchange resin included in the membrane. The DC of the sample was 51.1%, which is 6% higher than that of a similar sample of the MA-41P membrane.

Table 2: Comparative table of structural characteristics of MA-41P anion-exchange membrane samples.

Parameter		Sample			
		Initial dry	***Initial water-saturated***	***Worked after EDI***	***Worked after ED***
Absolute intensity of a crystalline peak, $I_{c.abs}$, c.u.	1st peak	376.908±18.468	247.358±11.378 (34.37% ↓)	238.684±11.934 (36.67% ↓)	236.449±12.059 (37.27% ↓)
	2nd peak	149.684±7.035	107.105±5.141 (28.45% ↓)	84.286±4.046 (43.69% ↓)	107.978±4.643 (27.86% ↓)
Half-width of a crystalline peak, *FWHM*, °	1st peak	0.430±0.021	0.5040±0.023 (17.21% ↑)	0.424±0.022 (1.40% ↓)	0.514±0.023 (19.53% ↑)
	2nd peak	0.642±0.033	0.859±0.040 (33.80% ↑)	0.673±0.031 (4.83% ↑)	0.807±0.038 (25.70% ↑)
Crystallite maximum size L_{max}, Å		3.474±0.153	2.958±0.148 (14.85% ↓)	3.517±0.176 (1.24% ↑)	2.908±0.147 (16.29% ↓)
Maximum intensity of an amorphous halo I_{am}, c.u.		59.989±2.879	50.792±2.590 (15.33% ↓)	52.349±2.670 (12.74% ↓)	42.869±1.929 (28.54% ↓)
Integral intensity of an amorphous halo $I_{am.i}$, c.u.		1193.199±53.694	1217.341±54.780 (2.02% ↑)	1325.577±62.302 (11.09% ↑)	1084.68±55.319 (9.09% ↓)
Common integral intensity $I_{com.i}$, c.u.		1737.337±83.392	1653.250±77.703 (4.84% ↓)	1684.549±84.227 (3.04% ↓)	1460.371±62.796 (15.94% ↓)

The water saturation process had the opposite effect on the cation-exchange membrane compared to the same process for the anion-exchange membrane. The crystalline peaks were shifted to the right to angles of 21.25 and 23.61°, and the interplanar distance decreased to 4.18 and 3.76 Å, respectively (Figure 6(b)). The areas with weakly expressed crystalline peaks were found in the intervals between 2θ angles from 33 to 37°, from 46 to 55°, and from 58 to 60°. The ranges of amorphous halos partially changed due to the saturation of the cation-exchange resin particles with moisture and were 12.5–37° and 37–60°, and the maximum intensity was slightly more than 55 conventional units. However, the DC of the sample changed insignificantly and was 50.9%.

The differences in the water saturation process of the cation-exchange membrane MK-40 from the anion-exchange membrane MA-41P can be explained by the small size and high hydrophilicity of the counterions contained in the cation-exchange membranes. Therefore, their structure can more effectively interact with water molecules, which contributes to faster activation of ion exchange [33].

The diffraction pattern of the working membrane sample after the EDI process (Figure 6(c)) is characterized by two crystalline peaks at 2θ angles of 21.79 and 24.23°, which indicates an even greater shift to the right than in the case of a water-saturated membrane, and a decrease in the interplanar distance of the crystallites to 4.10 and 3.69 Å. An increase in the intensity of two amorphous halos was also found, which is associated with the saturation of ion-exchange resins with components of the studied solutions in addition to moisture. The maximum intensity reached 65 c.u. The location intervals of both correspond to 2θ angles from 10 to 36° and from 36 to 60°. The DC of the sample significantly decreased to 39.52%.

The diffraction pattern of the working sample of the membrane after ED (Figure 6(d)) is characterized by the presence of two crystalline peaks at angles of 21.79 and 24.24°. A further shift of the peaks to the right compared to the previous samples is probably due to a stronger hydrodynamic effect on the membrane in the ED cell during the separation of solutions and subsequent compaction of the membrane. Regions with weakly expressed crystalline peaks were practically not detected, with the exception of a small area between angles of 36 and 37°. The DC of this working sample is higher than that of the sample after EDI and is 41.03%.

For the MK-40 membrane samples, after EDI and ED, there is a general decrease in the interplanar distance of the crystallites compared to the original samples. This is due to the gradual compaction of the membrane structure and a change in their properties as a result of cyclic operation. In addition, a denser structure leads to a change in the electrostatic fields inside the membrane. Ultimately, this can hinder the movement of ions and reduce the overall permeability of the membrane.

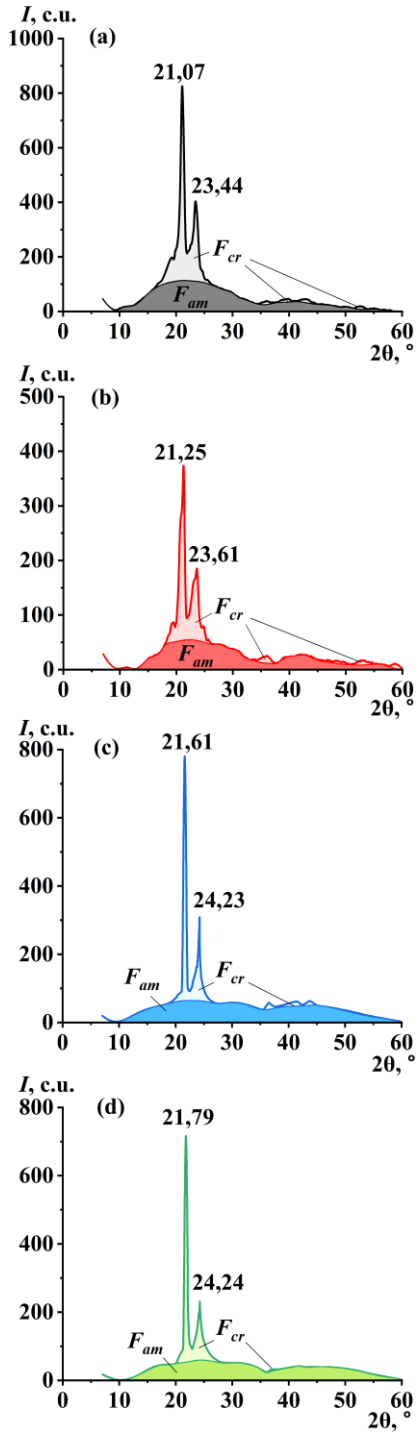

Figure 6: X-ray diffraction patterns of MK-40 membrane samples after background subtraction: *a* – initial dry; *b* – initial water-saturated; *c* – after EDI; *d* – after ED.

Table 3 shows the ratio of the main diffractometric parameters of the MK-40 membrane samples, which allows us to analyze and identify patterns of changes in the structure of the MK-40 cation-exchange membrane during EDI and ED. It should also be noted that both working membrane samples are characterized by an increase in intensity and a decrease in the width of crystalline peaks compared to the water-saturated sample. At the same time, a general decrease in these intensities is observed against the background of the diffractogram of the original dry sample. No such observations were noted for the MA-41P membrane samples.

As a result of the XRD research conducted, the following general conclusions can be drawn for both types of membranes. During the process of water saturation and operation of membranes in the EDI and ED processes for both types of ion-exchange membranes, in most cases, there is a decrease in the values of the main structural characteristics of the crystalline phase of the membranes (for example, the values of intensity and half-width of peaks, crystallite sizes). This is primarily due to defects and inhomogeneities in the crystalline phase of ion-exchange membranes due to the penetration of water molecules into the membrane structure and their interaction with the membrane components.

The observed deviation of diffraction angles in the diffraction patterns of membrane samples during water saturation and use in EDI and ED processes indicates the sensitivity of macromolecules to mechanical and thermal loads that arise under cyclic operation conditions. This is due to a change in structural ordering, amorphization of the polymer matrix and intermolecular interactions within the membrane structure.

Operation of membranes in the EDI process is characterized by a decrease in the membrane DC and an increase in their amorphous phase compared to the ED separation process, which contributes to better transfer of the corresponding ions through the membrane. The membranes themselves in this case are more susceptible to destruction and wear over time due to the effects of chemicals, which will ultimately lead to a decrease in their efficiency.

Table 3: Comparative table of structural characteristics of MK-40 anion-exchange membrane samples.

Parameter		Sample			
		Initial dry	***Initial water-saturated***	***Worked after EDI***	***Worked after ED***
Absolute intensity of a crystalline peak, $I_{c.abs}$, c.u.	1st peak	825.561±37.151	373.839±17.944 (54.72% ↓)	780.227±39.011 (5.49% ↓)	716.461±32.241 (13.22% ↓)
	2nd peak	403.547±18.563	185.164±8.703 (54.12% ↓)	308.865±13.590 (23.46% ↓)	231.258±11.794 (42.69% ↓)
Half-width of a crystalline peak, *FWHM*, °	1st peak	0.701±0.034	0.959±0.050 (36.80% ↑)	0.543±0.024 (22.54% ↓)	0.559±0.026 (20.26% ↓)
	2nd peak	0.930±0.046	1.246±0.053 (33.98% ↑)	0.384±0.019 (58.71% ↓)	0.690±0.032 (25.81% ↓)
Crystallite maximum size L_{max}, Å		2.118±0.106	1.551±0.081 (26.77% ↓)	3.957±0.202 (86.83% ↑)	2.670±0.134 (26.06% ↑)
Maximum intensity of an amorphous halo I_{am}, c.u.		115.733±5,092	55.178±2.759 (52.32% ↓)	65.422±3.009 (43.47% ↓)	57.951±2.666 (49.93% ↓)
Integral intensity of an amorphous halo $I_{am.i}$, c.u.		2311.675±97,090	1145.951±57.298 (50.43% ↓)	2068.492±88.945 (10.52% ↓)	1761.82±79.282 (23.79% ↓)
Common integral intensity $I_{com.i}$, c.u.		3655.203±175,450	1807.381±86.754 (50.55% ↓)	2819.943±121.258 (22.85% ↓)	2443.282±109.948 (33.16% ↓)

Comparative analysis of the structural characteristics of the studied membranes after EDI and ED allowed us to establish that the structure of the cation-exchange membrane MK-40 contains a greater percentage of the crystalline phase compared to the anion-exchange membrane MA-41P, which provides it with greater mechanical and chemical resistance during operation. In contrast, the anion-exchange membrane MA-41P is more amorphous and has a stronger absorption capacity.

The crystalline phase of ion-exchange membranes plays a key role in the ion transport process and their durability in industrial conditions. It determines the number of available paths for ion transport and can limit the movement of ions. This is due to the strictly ordered lattice compared to amorphous structures, which do not have such an order and provide freer channels for ion migration. The balance between these phases is key to optimizing the properties of ion-exchange membranes. The optimal ratio can make it possible to create membranes that combine high selectivity, and good permeability, have a long service life and withstand mechanical loads under operating conditions.

3.2 *Results of the DSC study*

Figure 7 shows DSC curves for samples of the MA-41P membrane. The initial section of the DSC curves from 30 to 100 °C is characterized by an endothermic reaction, which is caused by the release of moisture onto the surface of the samples and its subsequent evaporation.

The DSC curves in the temperature range of 130–137 °C showed a characteristic endothermic peak for all four membrane samples. This peak is due to the melting point of low-pressure (high-density) polyethylene, which is the binding polymer in the membrane structure [34]. The thermal effect ΔH for this peak on the DSC curves varied within the range of 1.448–4.841 J/g, with the highest being characteristic of the working membrane sample after the EDI process.

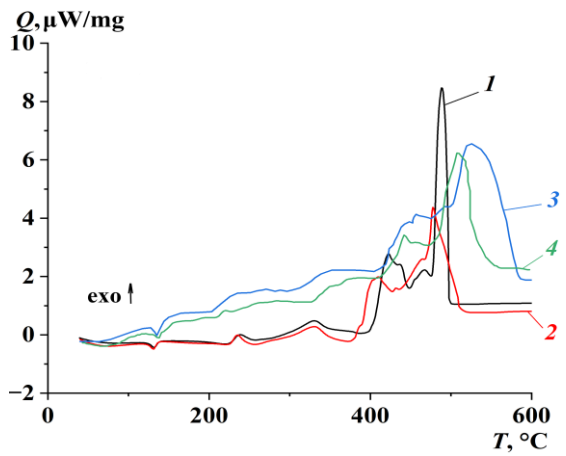

Figure 7: DSC curves of MA-41P membrane samples: *1* – initial dry; *2* – initial water-saturated; *3* – after EDI; *4* – after ED.

It should be noted that at temperatures above 65 °C, the heat flux released from 1 mg of sample mass for working membrane samples after EDI and ED begins to increase significantly compared to the initial dry and water-saturated samples. This is primarily due to the fact that these membrane samples absorbed some of the substances contained in the solutions being separated during EDI and ED. This resulted in an increase in sample mass and greater heat release [35].

In the temperature range of 218–240 °C, a clear exothermic peak with ΔH equal to 4.135 and 4.244 J/g is observed for the DSC curves of the initial dry and water-saturated samples. It is typical of polyamide used in the membrane production as a reinforcing material. However, for the working sample after EDI, an increase in the released energy is observed in the range from 210 to 230 °C, but the characteristic peak is not observed. For the membrane sample after ED, this peak is recorded, but it is less pronounced compared to the similar peak in the DSC curves of the initial samples. Its thermal effect ΔH is equal to 1.309 J/g. Probably, such differences between the initial and working samples are associated with the heterogeneity of the membrane thickness after the experiment.

The second half of the DSC curves after 300 °C is characterized by more intense reactions and processes associated with changes in the composition and structure of the membrane sample. There is a strong release of energy (the spread of ΔH for the samples varies within 218–414 J/g), which entails a loss of mass of the samples. This is due to the complete burnout of the carbon skeleton with the release of mainly CO_2, H_2O, CH_4. This is evidenced by the signals for the corresponding mass numbers. It should be emphasized that the DSC curves of the working membrane samples show a shift of all peaks in the above-mentioned region towards higher temperatures compared to the original samples.

The DSC curves for the MK-40 membrane samples are shown in Figure 8. The initial section of these dependencies up to 100 °C, as with the MA-41P membrane, is characterized by an endothermic reaction associated with the release of moisture onto the surface of the samples and its evaporation.

For the MK-40 membrane, it is necessary to note the fact that, unlike the MA-41P membrane, in this case, there is no significant increase in the heat flow on the DSC curves of the working samples after EDI and ED compared to the initial dry and water-saturated samples. This can be explained by the higher DC of the cation-exchange membrane, which entails a lower absorption capacity, as well as its greater mechanical and chemical resistance.

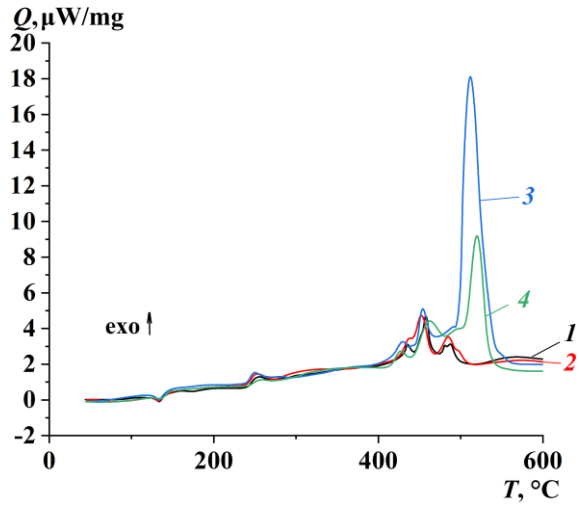

Figure 8: DSC curves of MK-40 membrane samples: *1* – initial dry; *2* – initial water-saturated; *3* – after EDI; *4* – after ED.

After a temperature of 100 °C, an endothermic peak standard for the MK-40 membrane is observed. It corresponds to the melting of polyethylene at temperatures from 132 to 134 °C, depending on the type of the membrane sample under study. The magnitude of the thermal effect ΔH from the melting of polyethylene for different membrane samples was small and did not exceed 5.561 J/g. In addition, a peak was recorded in the range of 248–256 °C, which, as in the case of the anion-exchange membrane, corresponds to polyamide. A greater thermal effect for this peak was found in the water-saturated sample and amounted to 11.366 J/g.

In the third section of the diagram at a temperature of over 400 °C, a large region is observed corresponding to the release of a significant amount of energy with a parallel loss of mass. In this case, the energy release characteristic of the working sample of the membrane after EDI is almost twice as large as that of the other samples. The thermal effect ΔH for this sample was 546.019 J/g. For the working samples of the membrane in this section, the observed greater energy surge is due to the release of adsorbed ions of heavy metals during the thermal destruction of ion-exchange resins, as well as the presence of defects in the crystalline phase of the membrane. The difference in the values of maximum temperatures, exothermic effects and half-widths of the peaks indicate different

chemical processes and phase transitions occurring in this section since the membranes were used to separate different solutions during EDI and ED.

4 Conclusions

EDI and ED processes use both anion-exchange and cation-exchange membranes to separate solutions from different types of ions. However, mechanical, chemical and thermal loads during the membrane operations in EDI and ED separation lead to the formation of different defects and the gradual destruction of the membrane structure. For example, the polymer matrix degradation and the formation of microcracks occur. These defects lead to a change in the anisotropic properties of the membrane and a violation of the ordering of ion-exchange groups. The membrane becomes less selective, the transmission of ions becomes less controllable, and undesirable reactions with the processed medium occur. In addition, due to the compaction of the membrane structure and the deformation of the interplanar distance of crystallites, a change in the dimension of ion transport channels is observed. These changes lead to a decrease in the selectivity of the membrane with respect to certain ions. These differences in the structural characteristics of the membranes under study are significant for their practical application in various processes. The cation-exchange membrane MK-40, due to its more crystalline structure, is more often used for tasks requiring membrane stability and durability. The anion-exchange membrane MA-41P is used in processes where high absorption capacity and interaction with ionic solutions are important.

In conclusion, it should be noted that the experimental data obtained as a result of the work demonstrate structural transformations of amorphous and crystalline phases in heterogeneous ion-exchange membranes MA-41P and MK-40 during repeated use for EDI and ED separation of multicomponent solutions. Understanding these transformations is important since more amorphous structures can provide better conditions for ion transport compared to crystalline ones. The obtained data will contribute to the development of membranes with high ion conductivity and selectivity, and further study of membrane material degradation. This will ultimately improve their durability and membrane efficiency under various operating conditions. This aspect is critically important for fuel cells, water purification and demineralization systems, as well as other industrial and scientific applications of ion-exchange membranes.

Acknowledgments

The work was prepared within the framework of the state assignment of the Ministry of Science and Higher Education of the Russian Federation, project No. FEMU-2024-0011.

Author contributions

S.L.: conception, data analysis, review and editing; K.V.: investigation, data analysis, manuscript writing, review and editing; I.Kh.: study design, data analysis, review and editing; M.M.: investigation, data analysis. All authors have read and agreed to the published version of the manuscript.

Conflict of Interest

The authors declare that they have no conflict of interest.

References

[1] D. S. Kudashova, N. A. Kononenko, M. A. Brovkina, and I. V. Falina, “A study of the degradation of a perfluorinated membrane during operation in a proton-exchange membrane fuel cell,” *Membranes and Membrane Technologies*, vol. 4, no. 1, pp. 23–30, Aug. 2022, doi: 10.1134/S251775162201005X.

[2] F. Guangul and G. Chala, “A comparative study between the seven types of fuel cells,” *Applied Science and Engineering Progress*, vol. 13, no. 3, pp. 185–194, Jul. 2020, doi: 10.14416/j.asep. 2020.04.007.

[3] T. A. Kravchenko, V. A. Krysanov, and I. A. Golovin “Nanosized complex of metal–ion-exchanger composites in the oxygen electrochemical reduction,” *Russian Journal of Electrochemistry*, vol. 59, no. 3, pp. 182–189, Mar. 2023, doi: 10.1134/s1023193523030059.

[4] M. Bdiri, C. Larchet, and L. Dammak, “A review on ion-exchange membranes fouling and antifouling during electrodialysis used in food industry: Cleanings and strategies of prevention,” *Chemistry Africa*, vol. 3, pp. 609–633, Aug. 2020, doi: 10.1007/s42250-020-00178-9.

[5] G. D. Gebreeyessus, "Status of hybrid membrane–ion-exchange systems for desalination: A comprehensive review," *Applied Water Science*, vol. 9, no. 135, Jul. 2019, doi: 10.1007/s13201-019-1006-9.

[6] M. Norrrahim, N. Kasim, V. Knight, K. Ong, S. Noor, S. Jamal, N. Shah, N. Halim, R. Ilyas, and W. Yunus, "Cationic nanocellulose as promising candidate for filtration material of COVID-19: A perspective" *Applied Science and Engineering Progress*, vol. 14, no. 4, pp. 580–587, Aug. 2021, doi: 10.14416/j.asep.2021.08.004.

[7] N. V. Loza, N. A. Kutenko, M. A. Brovkina, A. A. Samkov, and M. N. Kruglova, "The effect of lactose on the transport properties of ion-exchange membranes," *Membranes and Membrane Technologies*, vol. 13, no. 4, pp. 301–311, Apr. 2023, doi: 10.31857/S2218117223040041.

[8] M. Hoque, A. Rayhan, and S. Shaily, "Natural fiber-based green composites: Processing, properties and biomedical applications" *Applied Science and Engineering Progress*, vol. 14, no. 4, pp. 689–718, 2021, doi: 10.14416/j.asep.2021.09.005.

[9] A. Yaroslavtsev and V. Nikonenko, "Ion-exchange membrane materials: Properties, modification, and practical application," *Nanotechnologies in Russia*, vol. 4, no. 3–4, pp. 137–159, Apr. 2009, doi: 10.1134/S199507800903001X.

[10] Z. Yao, L. Hong-fei, A. Li-jia, and S. Jiang, "Progress in studies on structure and relaxation behavior of the amorphous phases in crystalline polymers," *Acta Polymerica Sinica*, vol. 013, no. 4, pp. 462–472, Apr. 2013, doi: 10.3724/SP.J.1105.2013.12362.

[11] L. Han, "Aging and degradation of ion-exchange membranes," in *Membrane Technology Enhancement for Environmental Protection and Sustainable Industrial Growth. Advances in Science, Technology & Innovation*, Z. Zhang, W. Zhang, and M. M. Chehimi, Eds. Cham: Springer, pp. 27–38, 2020.

[12] D. Mileva, D. Tranchida, and M. Gahleitner, "Designing polymer crystallinity: An industrial perspective," *Polymer Crystallization*, vol. 1, pp. 1–16, Apr. 2018, doi: 10.1002/pcr2.10009.

[13] L. Dammak, J. Fouilloux, M. Bdiri, C. Larchet, E. Renard, L. Baklouti, V. Sarapulova, A. Kozmai, and N. Pismenskaya, "A review on ion-exchange membrane fouling during the electrodialysis process in the food industry, part 1: Types, effects, characterization methods, fouling mechanisms and interactions," *Membranes*, vol. 11, no. 10, pp. 1–37, Oct. 2021, Art. no. 789, doi: 10.3390/membranes11100789.

[14] F. Tarasi, M. Medraj, A. Dolatabadi, J. Oberste-Berghaus, and C. Moreau, "Amorphous and crystalline phase formation during suspension plasma spraying of the alumina-zirconia composite," *Journal of the European Ceramic Society*, vol. 31, no. 15, pp. 2903–2913, Dec. 2011, doi: 10.1016/j.jeurceramsoc.2011.06.008.

[15] N. Koba de Moura, I. Siqueira, J. Machado, H. Kido, I. Avanzi, A. Rennó, E. Triches, and F. Passador, "Production and characterization of porous polymeric membranes of PLA/PCL blends with the addition of hydroxyapatite," *Journal of Composites Science*, vol. 3, no. 2, pp. 1–14, May 2019, doi: 10.3390/jcs3020045.

[16] M. Gaurav, D. M. Kalyon, F. T. Fisher, "Membranes of polyvinylidene fluoride and pvdf nanocomposites with carbon nanotubes via immersion precipitation," *Journal of Nanomaterials*, vol. 2008, no. 1, pp. 1–8, May 2008, doi: 10.1155/2008/759825.

[17] M. Ulaganathan, R. Nithya, and S. Rajendr, "Surface analysis studies on polymer electrolyte membranes using scanning electron microscope and atomic force microscope," in *Scanning Electron Microscopy*, V. Kazmiruk, Ed. London: InTech, pp. 671–694, 2012.

[18] S. Abbrent and S. Greenbaum, "Using nuclear magnetic resonance spectroscopy in polymer electrolyte research," in *Polymer Electrolytes*, C. Sequeira and D. Santos, Ed. Cambridge: Woodhead Publishing, pp. 278–313, 2010.

[19] T. Agarwal, A. Prasad, S. Advani, S. Komini Babu, and R. Borup, "Review: Infrared spectroscopy for understanding the structure of nafion and its associated properties," *Journal of Materials Chemistry A*, vol. 12, no. 4, pp. 1–34, Apr. 2024, 10.1039/D3TA05653H.

[20] E. Gusev, A. Dedkova, and N. Djuzhev, "Investigating mechanical strength of multilayer membranes for MEMS converters of physical quantities," *Nanoindustry Russia*, pp. 538–541, Jan. 2018, doi: 10.22184/1993-8578.2018.82.538.541.

[21] A. Basile and F. Gallucci, *Membranes for Membrane Reactors: Preparation, Optimization and Selection*. Chichester: Wiley, p. 615, 2011.

[22] P. Y. Apel, O. V. Bobreshova, A. V. Volkov, V. V. Volkov, V. V. Nikonenko, I. A. Stenina, A.

N. Filippov, Y. P. Yampolskii, and A. B. Yaroslavtsev, "Prospects of Membrane Science Development," *Membranes and Membrane Technologies*, vol. 1, pp. 45–63, May 2019, doi: 10.1134/S2517751619020021.

[23] I. Oladele, T. Omotosho, G. Ogunwande, and F. Adebayo, "A review on the philosophies for the advancement of polymer-based composites: Past, present and future perspective," *Applied Science and Engineering Progress*, vol. 14, no. 4, pp. 553–579, Aug. 2021, doi: 10.14416/j.asep.2021.08.003.

[24] Azotom, "Shchekinoazot. Monopolar membranes" 2024. [Online]. Available: http://www.azotom.ru/monopolyarnye-membrany/

[25] V. I. Zabolotskii, S. A. Loza, and M. V. Sharafan, "Physicochemical properties of profiled heterogeneous ion-exchange membranes," *Russian Journal of Electrochemistry*, vol. 41, no. 10, pp. 1053–1060, Oct. 2005, doi: 10.1007/s11175-005-0180-2.

[26] W. H. Bragg and W. L. Bragg, "The reflection of X-rays by crystals," *Proceedings of the Royal Society of London. Series A*, vol. 88, pp. 428–438, Jul. 1913, doi: 10.1098/rspa.1913.0040

[27] A. K. Chatterjee, "X-Ray Diffraction" in *Handbook of Analytical Techniques in Concrete Science and Technology*, V. Ramachandran and J. Beaudoin, Ed. Amsterdam, Netherlands: Elsevier, pp. 275–332, 2001.

[28] B. Lavina, P. Dera, and R. T. Downs, "Modern x-ray diffraction methods in mineralogy and geosciences," *Reviews in Mineralogy and Geochemistry*, vol. 78, no. 1, pp. 1–31, Jan. 2014, doi: 10.2138/rmg.2014.78.1

[29] S. L. Aggarwal and G. P. Tilley, "Determination of crystallinity in polyethylene by X-ray diffractometer," *Journal of Polymer Science*, vol. 18, no. 87, pp. 17–26, Sep. 1955, doi: 10.1002/pol.1955.120188702

[30] M. Martynov and K. Vylegzhanina, *Polymer Radiography: Workbook for Industrial Laboratories*. Leningrad: Khimiya, p. 96, 1972.

[31] A. Zatirakha, A. Smolenkov, A. Pirogov, P. Nesterenko, and O. Shpigun, "Preparation and characterisation of anion exchangers with dihydroxy-containing alkyl substitutes in the quaternary ammonium functional groups," *Journal of Chromatography A*, vol. 1323, no. 104–114, pp. 1–32, Jan. 2014, doi: 10.1016/j.chroma.2013.11.013.

[32] S. L. Price, "Predicting crystal structures of organic compounds," *Chemical Society Reviews*, vol. 43, no. 7, pp. 2098–2111, Apr. 2014, doi: 10.1039/C3CS60279F

[33] N. Maiygurova, F. Rößner, T. Eliseeva, and V. Selemenev, "Sorption of amino acid and changes in hydration of heterogeneous cation- and anion-exchange membranes Fumasep," *Izvestiya Vysshikh Uchebnykh Zavedeniy. Khimiya Khimicheskaya Tekhnologiya*, vol. 59, no. 4, pp. 73–77, Apr. 2016, doi: 10.6060/tcct.20165904.5336.

[34] D. Malpass, *Introduction to Industrial Polyethylene: Properties, Catalysts, and Processes. Introduction to Industrial Polyethylene: Properties, Catalysts, and Processes*. Salem: Wiley-Scrivener, p. 156, 2010.

[35] M. Bernhard, N. Fuchs, P. Presoly, P. Angerer, B. Friessnegger, and C. Bernhard, "Characterization of the γ-loop in the Fe P system by coupling DSC and HT-LSCM with complementary in-situ experimental techniques," *Materials Characterization*, vol. 174, pp. 1–17, Feb. 2021, doi: 10.1016/j.matchar.2021.111030.